Article

Cell Reports

Nat1 Deficiency Is Associated with Mitochondrial Dysfunction and Exercise Intolerance in Mice

Graphical Abstract

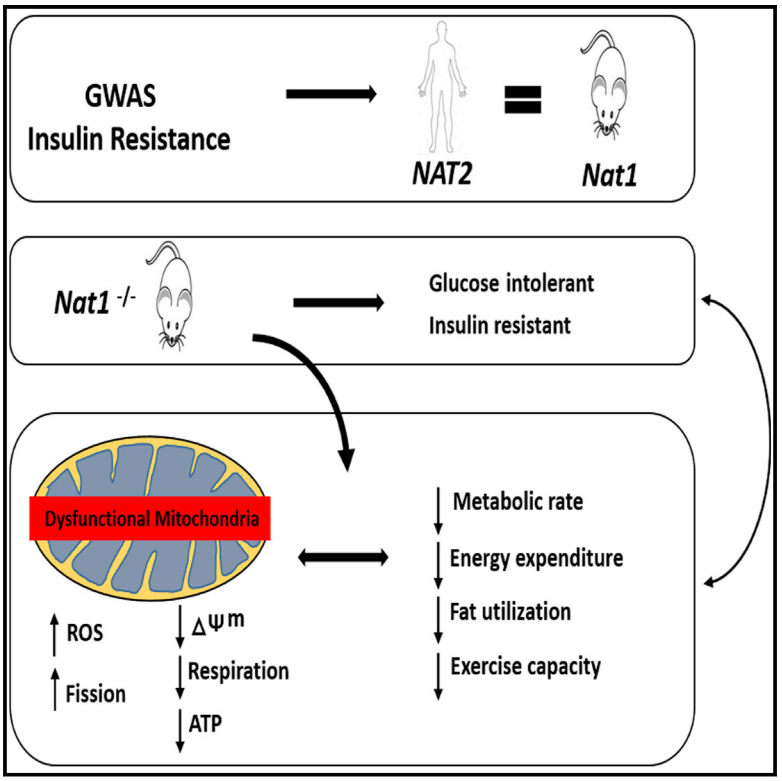

Authors

Indumathi Chennamsetty, Michael Coronado, Kévin Contrepois, ..., Daniel Bernstein, Thomas Quertermous, Joshua W. Knowles

Correspondence

knowlej@stanford.edu

In Brief

Chennamsetty et al. show that deficiency of *Nat1* (ortholog of the human insulin resistance gene *NAT2*) decreases mitochondrial function in vitro and in vivo. *Nat1*-deficient mice have decreased basal respiration, maximal exercise capacity, and the ability to utilize fat for energy.

Highlights

- Absence of the insulin resistance gene *Nat1* results in mitochondrial dysfunction
- *Nat1* deficiency in mice is associated with a decreased ability to utilize fats for energy
- *Nat1*-deficient mice have decreased basal metabolic rate and exercise capacity

Chennamsetty et al., 2016, Cell Reports *17*, 527–540
October 4, 2016
http://dx.doi.org/10.1016/j.celrep.2016.09.005

Cell Reports
Article

Nat1 Deficiency Is Associated with Mitochondrial Dysfunction and Exercise Intolerance in Mice

Indumathi Chennamsetty,[1] Michael Coronado,[2] Kévin Contrepois,[3] Mark P. Keller,[4] Ivan Carcamo-Orive,[1] John Sandin,[1] Giovanni Fajardo,[2] Andrew J. Whittle,[5] Mohsen Fathzadeh,[1] Michael Snyder,[3] Gerald Reaven,[1] Alan D. Attie,[4] Daniel Bernstein,[2] Thomas Quertermous,[1] and Joshua W. Knowles[1,6,*]
[1]Division of Cardiovascular Medicine and Cardiovascular Institute, Stanford University School of Medicine, Stanford, CA 94305, USA
[2]Division of Cardiology, Department of Pediatrics, Stanford University, Stanford, CA 94305, USA
[3]Department of Genetics, Stanford University School of Medicine, Stanford, CA 94305, USA
[4]Department of Biochemistry, University of Wisconsin, Madison, WI 53706, USA
[5]Department of Psychiatry, Stanford University, Stanford, CA 94305, USA
[6]Lead Contact
*Correspondence: knowlej@stanford.edu
http://dx.doi.org/10.1016/j.celrep.2016.09.005

SUMMARY

We recently identified human N-acetyltransferase 2 (*NAT2*) as an insulin resistance (IR) gene. Here, we examine the cellular mechanism linking *NAT2* to IR and find that *Nat1* (mouse ortholog of *NAT2*) is co-regulated with key mitochondrial genes. RNAi-mediated silencing of *Nat1* led to mitochondrial dysfunction characterized by increased intracellular reactive oxygen species and mitochondrial fragmentation as well as decreased mitochondrial membrane potential, biogenesis, mass, cellular respiration, and ATP generation. These effects were consistent in 3T3-L1 adipocytes, C2C12 myoblasts, and in tissues from *Nat1*-deficient mice, including white adipose tissue, heart, and skeletal muscle. *Nat1*-deficient mice had changes in plasma metabolites and lipids consistent with a decreased ability to utilize fats for energy and a decrease in basal metabolic rate and exercise capacity without altered thermogenesis. Collectively, our results suggest that *Nat1* deficiency results in mitochondrial dysfunction, which may constitute a mechanistic link between this gene and IR.

INTRODUCTION

The worldwide prevalence of insulin resistance (IR) and its metabolic complications have increased substantially in recent decades (Facchini et al., 2001; Frayn, 2001; Reaven, 1988; Yip et al., 1998). It is estimated that 25% to 33% of the USA population is sufficiently insulin resistant to be at risk for adverse clinical consequences. At a tissue level, while decreased insulin-mediated glucose uptake in skeletal muscle is a cardinal feature of IR, it is also apparent that IR and dysfunctional adipose tissue are inextricably intertwined and co-occur in type 2 diabetes mellitus (T2D) and cardiovascular disease (Kim et al., 2007; Wang et al., 2005; Weyer et al., 2000). Hallmarks of IR in adipose tissue include decreased insulin-mediated glucose uptake, inability of insulin to suppress lipolysis, dysregulation of adipocyte growth and differentiation, mitochondrial dysfunction, disrupted adipokine signaling, and, in some instances, increased inflammation (De Pauw et al., 2009). Nevertheless, the genetic and cellular mechanisms underlying IR in adipose tissue remain incompletely understood.

We recently identified an association of non-synonymous coding SNPs in the human N-acetyltransferase 2 (*NAT2*) gene with IR using a genome-wide association study (GWAS) approach, and we validated these findings in vitro and in vivo through perturbations of the murine ortholog *Nat1*. In the murine 3T3-L1 adipocyte cell line, silencing *Nat1* decreased insulin-mediated glucose uptake and increased basal and isoproterenol-stimulated lipolysis. *Nat1*-deficient mice had elevated fasting blood glucose, insulin, and triglyceride levels and decreased insulin sensitivity, as measured by glucose and insulin tolerance tests (Knowles et al., 2015). The exact mechanism linking the association of *Nat1* with IR remains unclear, and identification of the missing link among *Nat1*, insulin action, and cellular metabolism in adipose tissue is an important next step toward our understanding of the actions of this gene.

Here, we show that *Nat1* is not only strongly co-regulated with key mitochondrial genes but also that *Nat1* deficiency causes significant decreases in multiple indices of mitochondrial function in vitro as well as global lipid metabolism alterations in vivo. Furthermore, *Nat1*-deficient mice have a marked decrease in basal metabolic rate and exercise capacity. Taken together, these data suggest that mitochondrial dysfunction may be a cellular mechanistic link among *Nat1*, insulin sensitivity, and whole-body energy expenditure.

RESULTS

Characterization of *Nat1*-Deficient Mice on Regular Chow

A significant increase in mean body weight was observed in the *Nat1* knockout (*Nat1* KO) mice compared to their wild-type (WT) littermate controls after 15 weeks on a regular chow diet (Figure 1A), despite no difference in food or water intake (data not

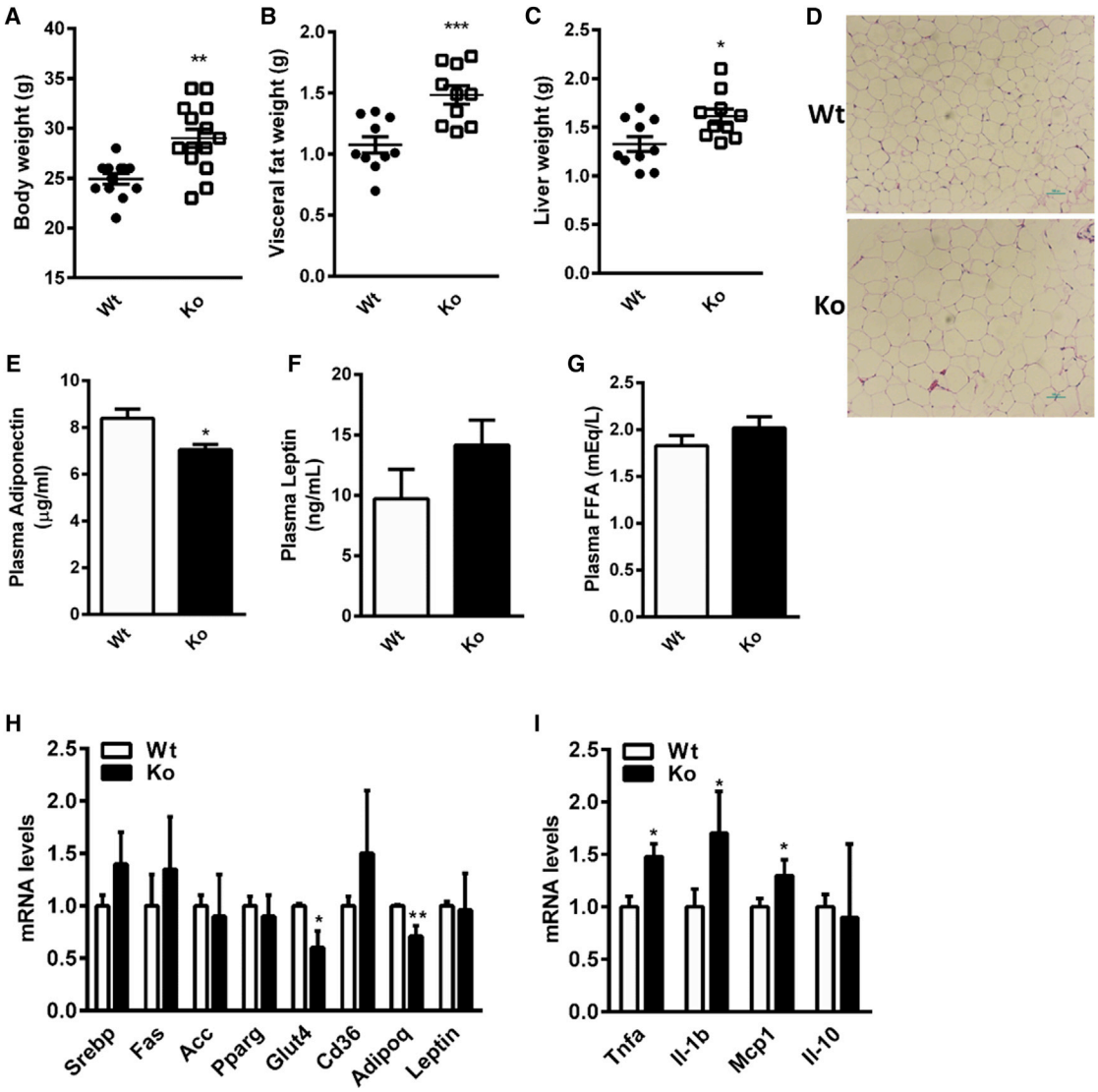

Figure 1. Metabolic Characterization of *Nat1*-Deficient Mice

(A–C) Body weight (A), epididymal fat (B), and liver weights (C) of wild-type (WT) and *Nat1*-deficient mice (KO) at 16 weeks fed a chow diet (n = 10–15 mice per group). Values are mean ± SEM.

(D) H&E staining of epididymal WAT of WT and *Nat1*-deficient mice is shown. Scale bar, 100 Pi (10× magnification).

(E–G) Plasma adiponectin (E), leptin (F), and FFA concentrations (G) were determined in mice fasted overnight (n = 10–13 per genotype). Values represent means ± SEM (***$p \leq 0.001$, **$p \leq 0.01$, and *$p < 0.05$).

(H and I) Gene expression profiling in WAT in WT and *Nat1* KO mice (n = 5–6 mice per group) using real-time qPCR for expression of genes involved in lipid metabolism (H) and for inflammatory markers (I). The expression values were normalized to cyclophilin. Results represent mean ± SEM (**$p \leq 0.01$ and *$p < 0.05$).

shown). The weights of epididymal fat and liver were significantly increased in *Nat1* KO mice compared to those of the control mice (Figures 1B and 1C), and H&E staining of epididymal fat tissue revealed that *Nat1*-deficient mice exhibit larger adipocytes compared to the WT controls (Figure 1D). The increased adiposity in *Nat1* KO mice was accompanied by a decrease in the adipose expression of adiponectin (*Adipoq*), mirrored by a 17% decrease in plasma adiponectin levels (Figure 1E), while there was a non-significant increase in plasma leptin levels (Figure 1F). Livers of *Nat1*-deficient mice exhibited increased intrahepatic triglyceride content on regular chow (Figures S1A and S1B) compared with control mice. No differences were observed in liver enzymes (Figures S1C and S1D).

Free fatty acid (FFA) concentrations were comparable between *Nat1* KO and WT mice (Figure 1G), despite elevated plasma triacylglycerol (TG) levels in the *Nat1* KO mice (Knowles et al., 2015). The mRNA levels of important genes involved in lipogenesis and FFA transport (e.g., *Srebp1*, *Fas*, and *Cd36*) were not significantly elevated in *Nat1*-deficient mice. As expected given the decreased insulin sensitivity observed in *Nat1* KO mice, the expression of *Glut4* was also significantly decreased in *Nat1* KO mice (Figure 1H).

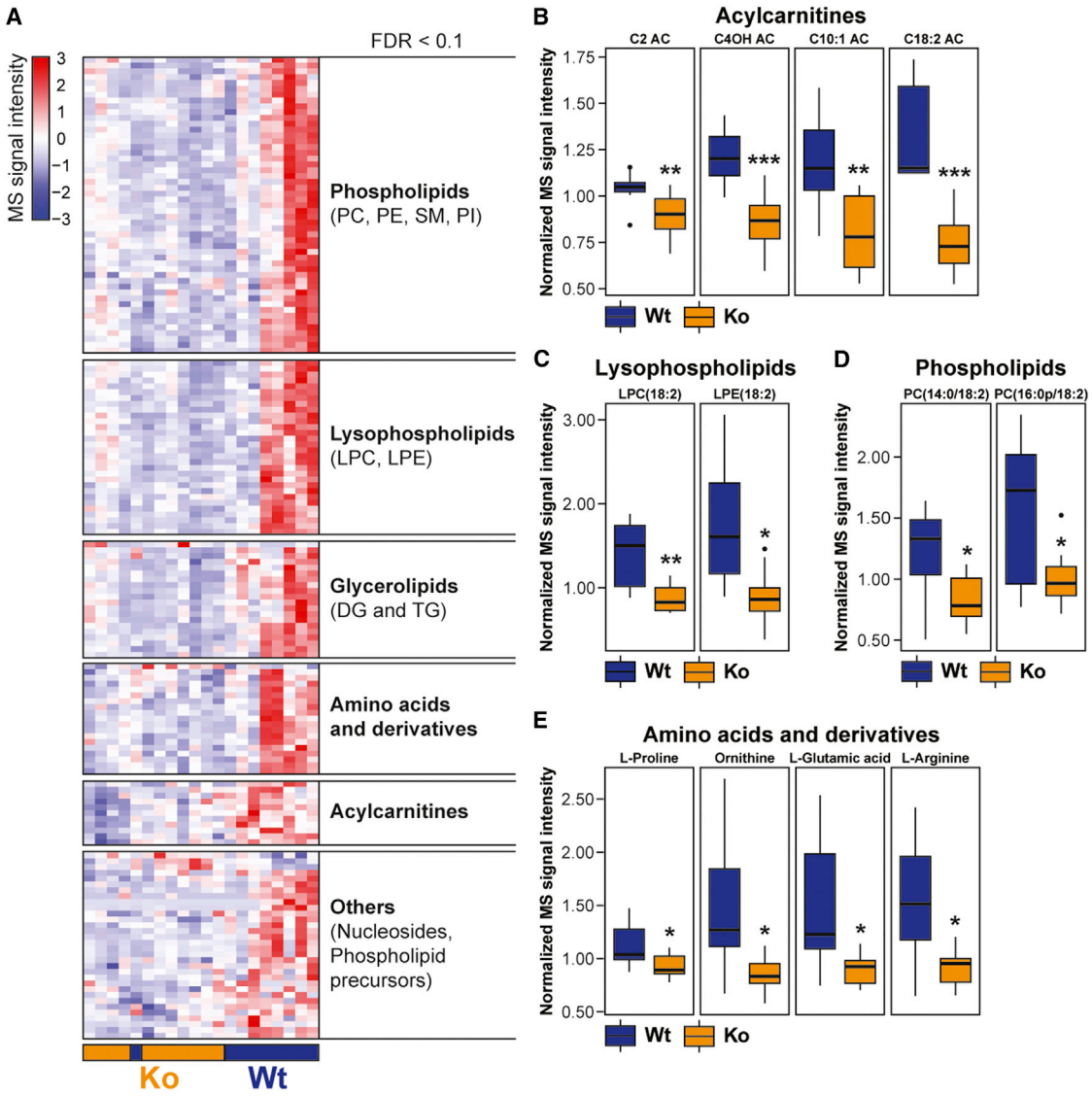

Figure 2. Effect of *Nat1* Deficiency on Fasting Plasma Metabolome and Lipidome

(A) Hierarchical clustering of significantly different metabolites and lipids in fasting plasma from non-targeted metabolomics and lipidomics experiments (FDR < 0.1). Signal intensities were clustered in two dimensions (horizontal, metabolites and lipids; vertical, samples) on the basis of Euclidean distance. Colors indicate metabolite/lipid abundance as high (red), median (white), or low (blue).

(B–E) Values are normalized to the median and expressed as box-and-whisker plots (n = 9–11; *p ≤ 0.05, **p ≤ 0.01, and ***p ≤ 0.001). AC, acylcarnitine; DG, diacylglycerol; PC, phosphatidylcholine; PE, phosphatidylethanolamine; PI, phosphatidylinositol; SM, sphingomyelin; TG, triacylglycerol. The list of significantly changing metabolites and lipids is given in Table S1. Data obtained from non-fasting plasma samples are shown in Figure S2.

In addition, we found increased expression of the pro-inflammatory markers *Tnfa*, *Il-1b*, and *Mcp1* (*Ccl2*) in adipose tissue of *Nat1* KO mice compared to WT littermates (Figure 1I), whereas there was no difference in the *Il-10* expression levels between the groups.

Effects of *Nat1* Deficiency on Plasma Metabolome and Lipidome

We performed a comprehensive metabolite and lipid profiling of fasting plasma from WT and *Nat1* KO mice using a broad-spectrum liquid chromatography coupled with mass spectrometry platform (Contrepois et al., 2015). Comparative analysis of the metabolites and lipids revealed that lipid metabolism was profoundly perturbed in *Nat1* KO mice compared to the WT littermate controls. In particular, the plasma levels of 51 phospholipids, 30 lysophospholipids, 20 glycerolipids, and 11 acylcarnitines were decreased in *Nat1* KO mice compared to WT littermate mice (Figure 2A). Similar changes were observed in non-fasting plasma, despite more inter-individual variability due to small differences in postprandial timing after which the blood was drawn (Figure S2).

Short-chain (C2, C4OH, C6, and C6DC), medium-chain (C10:1 and C10:3), and long-chain (C14, C14:2, C16:0, C18:1, and

C18:2) acylcarnitines, intermediates of fatty acid oxidation, were diminished in the plasma of *Nat1* KO mice, suggesting remodeling of the oxidative phosphorylation (OXPHOS) process and changes in lipid oxidation (Figure 2B). Interestingly, most of the significantly deregulated lipids contained essential linoleic acid (18:2), such as lysophosphatidylcholine (LPC) (18:2), lysophosphatidylethanolamine (LPE) (18:2), phosphatidylcholine (PC) (14:0/18:2), PC (16:0p/18:2), TG (18:2/20:4/22:6), and TG (18:3/18:2/22:6) (Figures 2C and 2D; Table S1). In addition to lipid metabolism, 19 amino acids and derivatives were significantly reduced in *Nat1*-deficient mice. Pathway analysis revealed a significant alteration of arginine and proline metabolism (false discovery rate [FDR] = 0.0035), among which L-proline, ornithine, L-glutamic acid, and L-arginine are key metabolites (Figure 2E). Glycine, serine, and threonine metabolism also was significantly altered (FDR = 0.0301). Interestingly, derivatives of L-arginine (homoarginine, N,N-dimethylarginine) along with L-lysine and N6-acetyl-L-lysine also were significantly decreased. An exhaustive list of the metabolites and lipids significantly altered upon *Nat1* knockdown can be found in Table S1.

Nat1 Expression in Adipose Is Co-regulated with Mitochondrial Genes

To provide insight into the metabolic pathways interacting with *Nat1*, we examined co-expression gene networks in adipose tissue collected from a large mouse cohort that segregated for obesity-induced diabetes (Tian et al., 2015; Tu et al., 2012). Gene ontology (GO) and Kyoto Encyclopedia of Genes and Genomes (KEGG) pathway analyses were performed to identify the molecular functions and biological processes of genes that correlated with *Nat1* expression. Interestingly, genes that positively correlated with *Nat1* expression were significantly enriched for biological processes associated with mitochondrial biology, glucose metabolism, and energy balance (Figures S3A and S3B). Genes that negatively correlated with *Nat1* expression in adipose significantly enriched for growth factor binding and extracellular matrix (Figure S3C). The list of mitochondrial genes most positively correlated with *Nat1* expression in adipose tissue is shown in Table S2.

Loss of *Nat1* Decreases Mitochondrial Function in 3T3-L1 Adipocytes

Based on data indicating that *Nat1* is strongly co-regulated with mitochondrial pathway genes, we sought to comprehensively evaluate mitochondrial function resulting from the perturbations of *Nat1*. Increased reactive oxygen species (ROS) production is often observed in mitochondrial dysfunction and IR (Sivitz and Yorek, 2010). ROS was measured using 2′,7′-dichlorodihydrofluorescein diacetate (H2DCFDA). Knockdown of *Nat1* in 3T3-L1 adipocytes markedly induced ROS production (~1.3-fold) and strongly elevated the production of mitochondrial superoxide (O_2^-), a major source of mitochondrial ROS when evaluated with Mitosox Red (Figures 3A and 3B). Because the electrochemical gradient of the mitochondrial membrane is essential for ATP synthesis, we monitored mitochondrial membrane potential by fluorescence microscopy. Cells were stained with Tetramethylrhodamine methyl ester (TMRM), imaged with a fluorescent microscope, and the intensity of TMRM fluorescence was determined (Figure 3C). We found that *Nat1* silencing resulted in a decrease of mitochondrial membrane potential of ~30%, suggesting that loss of *Nat1* markedly induced mitochondrial membrane depolarization in adipocytes from 3T3-L1 cells. Loss of membrane potential was further verified using a fluorescent plate reader, which showed a decreased membrane potential of ~30% (Figure 3D).

Nat1 Deficiency Decreases Mitochondrial Mass and Biogenesis in Adipocytes

To explore whether the loss of *Nat1* affects mitochondrial number and biogenesis, we measured mitochondrial mass using a fluorescent probe, MitoTracker deep red. Intensity of MitoTracker fluorescence was analyzed by flow cytometry and was further verified by confocal imaging (Figures 3E and 3F). Loss of *Nat1* significantly decreased mitochondrial mass by 22%. We then measured the expression of peroxisome proliferator-activated receptor gamma coactivator-1-alpha (*Pgc1a*) (Ppargc1a), a transcriptional co-activator implicated in mitochondrial biogenesis and adaptive thermogenesis. *Pgc1a* was significantly downregulated at both mRNA and protein levels in the knockdown group compared to controls (Figures 3G and 3H). To further explore the changes in mitochondrial biogenesis and oxidative phosphorylation, we also assessed the levels of key regulators of mitochondria by real-time qPCR. *Nrf1*, *Tfam*, *Cycs*, and *Pgc1b* were significantly downregulated in the *Nat1* knockdown group compared to controls, which is consistent with the in vivo results (Figure 3I). Our findings suggest that the loss of *Nat1* decreases mitochondrial mass and biogenesis in 3T3-L1 adipocytes.

Given these findings, we also assessed the expression of genes involved in mitochondrial biogenesis and oxidative phosphorylation in white adipose tissue (WAT) of WT and *Nat1*-deficient mice. The deletion of *Nat1* significantly decreased the expression of *Pgc1a* and cytochrome *c* (*Cycs*) (Figure S3D).

Nat1 Knockdown Promotes Drp1-Dependent Mitochondrial Fragmentation

We evaluated the effect of *Nat1* knockdown on the regulation of mitochondrial dynamics by performing confocal microscopy on 3T3-L1 cells and assessing morphology with MitoTracker Red CMXRos. Mitochondrial fragmentation is a morphological phenotype normally associated with dysfunctional mitochondria, such as with ischemic reperfusion injury (Disatnik et al., 2013). We observed a marked increase in mitochondrial fragmentation in *Nat1* KO cells compared to the controls (Figure 4A). Mitochondrial fragmentation can occur by a number of mechanisms, including increased mitochondrial fission, decreased mitochondrial fusion, or decreased mitophagy (Dorn, 2015). We first examined dynamin 1-like protein (Drp1) (Dnm1l) expression in 3T3-L1 adipocytes by western blot, since Drp1 is the key regulator of mitochondrial fission. Knocking down *Nat1* in 3T3-L1 adipocytes led to a significant increase of Drp1 in the mitochondrial fraction by 1.6-fold (Figure 4B). We then measured the levels of the mitochondrial fusion proteins Mfn1 and Mfn2 and mitophagy proteins Lc3a/b and Pink1, and we found no difference between groups (Figures 4C and 4D).

We also measured mitochondrial markers in isolated mitochondrial fractions from WAT of WT and *Nat1*-deficient mice.

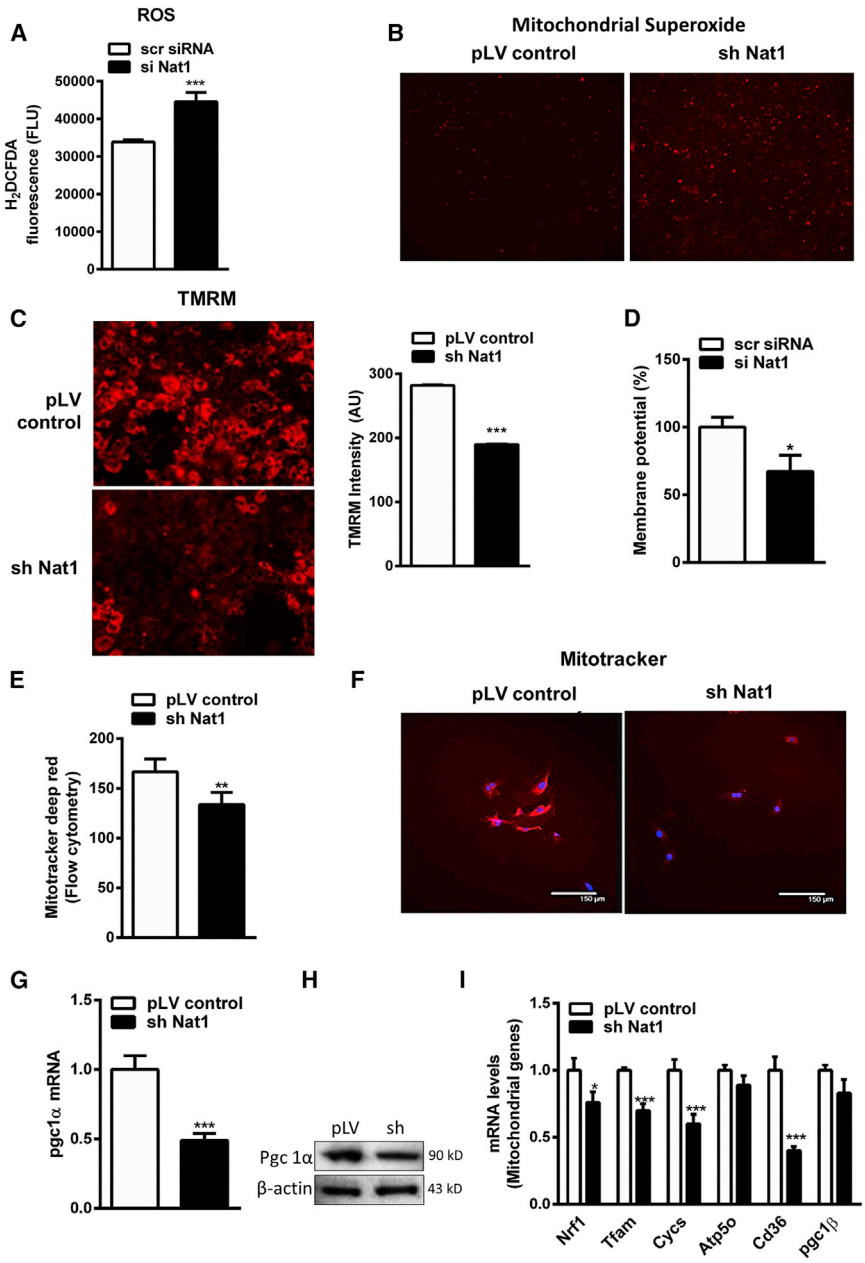

Figure 3. Effect of *Nat1* Knockdown on Mitochondrial Functions

(A) Intracellular ROS was measured using H2DCFDA in 3T3-L1 adipocytes transfected with scrambled siRNA (scr siRNA) or with siRNA against *Nat1* (si *Nat1*).

(B) Mitochondrial superoxides were measured by fluorescence microscopy in 3T3-L1 adipocytes transduced with lentiviral controls and sh *Nat1* stained with MitoSOX Red (10 μM) (4× magnification). Mitochondrial membrane potential (ΔΨm) was monitored using TMRM staining (50 nM) in 3T3-L1 adipocytes.

(C) Fluorescent microscopic analysis (20× magnification) and intensity of TMRM were quantified.

(D) Membrane potential was further analyzed using fluorescent plate reader. Data are presented as mean ± SEM of three separate experiments, with eight wells per condition. Mitochondrial mass was measured in 3T3-L1 adipocytes transduced with lentivirus controls and sh *Nat1* using MitoTracker deep red (100 nM).

(E) Fluorescence was analyzed by flow cytometry. Values are mean ± SEM of triplicates of three different experiments (**p ≤ 0.01).

(F) Confocal microscopy in 3T3-L1 adipocytes is shown.

(G) The qPCR analysis of *Pgc1a* expression in 3T3-L1 adipocytes. Data represent mean ± SEM.

(H) Western blot analysis of Pgc1a protein levels in differentiating mouse 3T3-L1 adipocytes is shown.

(I) The qPCR analysis of mitochondrial genes in 3T3-L1 adipocytes normalized to cyclophilin. Representative results are shown of three experiments. Data are presented as mean ± SEM (*p < 0.05, **p ≤ 0.01, and ***p < 0.001).

Nat1 deficiency increased Drp1 expression (Figure 4E). Electron microscopy of WAT showed smaller and more circular mitochondria in *Nat1* KO mice compared with WT mice (Figure S4).

Taken together, these data indicate that the deficiency of *Nat1* is associated with mitochondrial fragmentation mediated by Drp1-dependent mechanisms of mitochondrial fission and results in significant changes to the morphology and number of mitochondria, which also are observed in vivo.

Nat1 Silencing Decreases Cellular Respiration and ATP Generation in Adipocytes

Given that impaired mitochondrial respiration has been linked to the development of IR, we measured in situ respiratory capacity using the XF24 Seahorse extracellular flux analyzer with cultured adipocytes. Respiration rates were calculated as a function of changes in the oxygen consumption rate (OCR) in response to oligomycin, carbonyl cyanide 4-trifluoromethoxyphenylhydrazone (FCCP), and antimycin/rotenone. *Nat1*-silenced cells had a reduced OCR relative to control adipocytes (Figure 5A). The results of the respiration studies indicated that *Nat1* knockdown adipocytes had decreased basal and maximal respiration by 18% and 26%, respectively, compared to the control adipocytes (Figure 5B). Extracellular acidification rate (ECAR) also was measured as an index of lactate production. We found no difference in the basal acidification rate; however, the maximal acidification rate was decreased in *Nat1* knockdown adipocytes compared to the controls (Figures S5A and S5B).

Decreased cellular respiration was further verified in WAT of WT and *Nat1*-deficient mice using an Oroboros Oxygraph-2k respirometer. *Nat1* deficiency significantly decreased basal respiration (Figure 5C). Decreased OCR was accompanied by a significant decrease in mtDNA content in WAT of *Nat1*-deficient

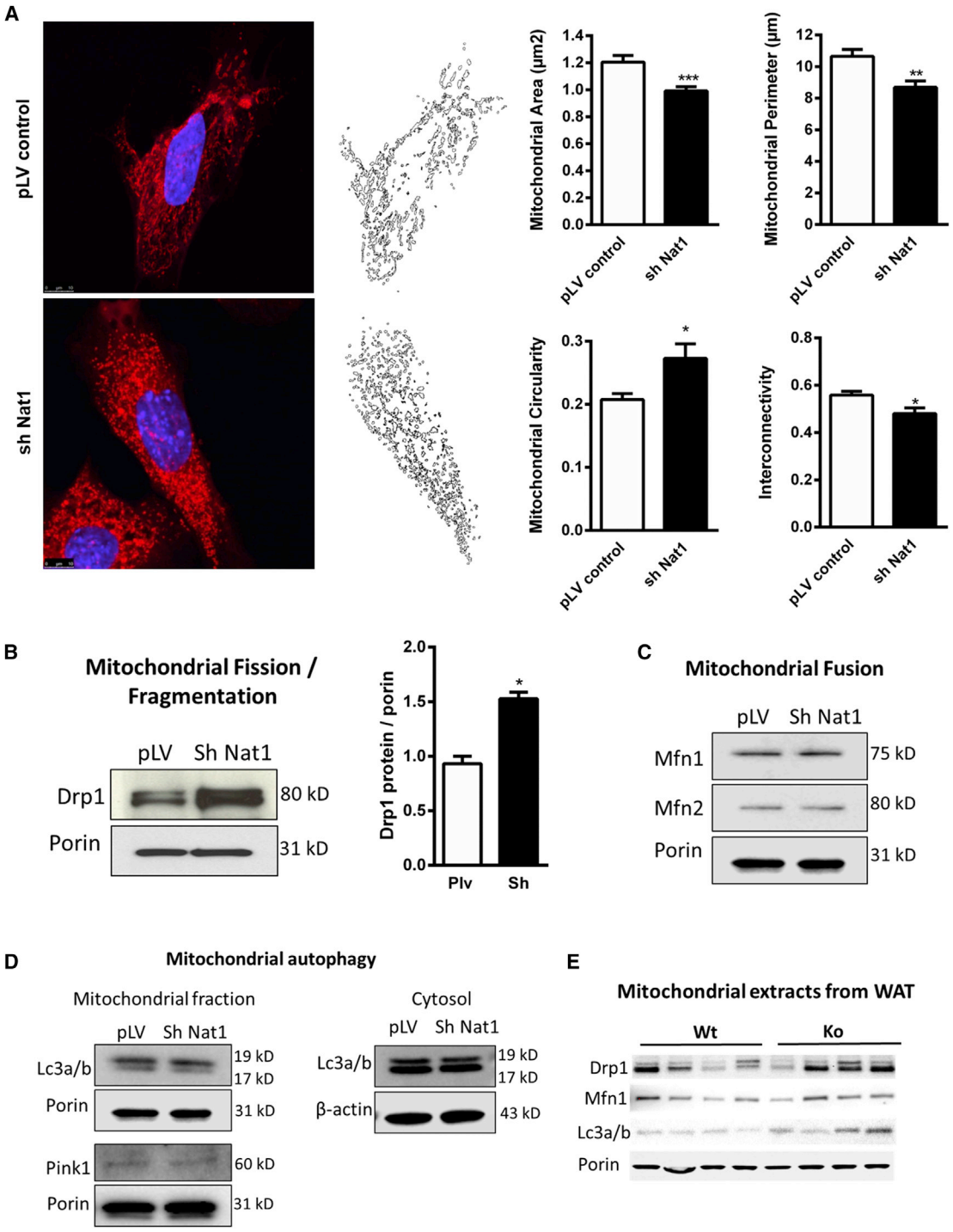

Figure 4. Effect of *Nat1* on Mitochondrial Dynamics in 3T3-L1 Adipocytes

Nat1 knockdown increased mitochondrial fission/fragmentation

(A) Confocal imaging shows mitochondrial fragmentation in 3T3-L1 adipocytes transduced with lentivirus for controls and sh *Nat1* stained with MitoTracker Red CMXRos (100 nM) and analyzed for mitochondrial area, perimeter, circularity, and interconnectivity.

(B) Western blot analysis of mitochondrial proteins for mitochondrial fission quantified by ImageJ. Values are mean ± SEM of two different experiments (*$p \leq 0.05$).

(C and D) Fusion (C) and mitophagy (D) in isolated mitochondrial and cytosolic fractions from 3T3-L1 adipocytes transduced with lentivirus for controls and sh *Nat1* are shown.

(E) Mitochondrial markers in isolated mitochondrial fractions from WAT of WT and *Nat1*-deficient mice are shown (n = 4).

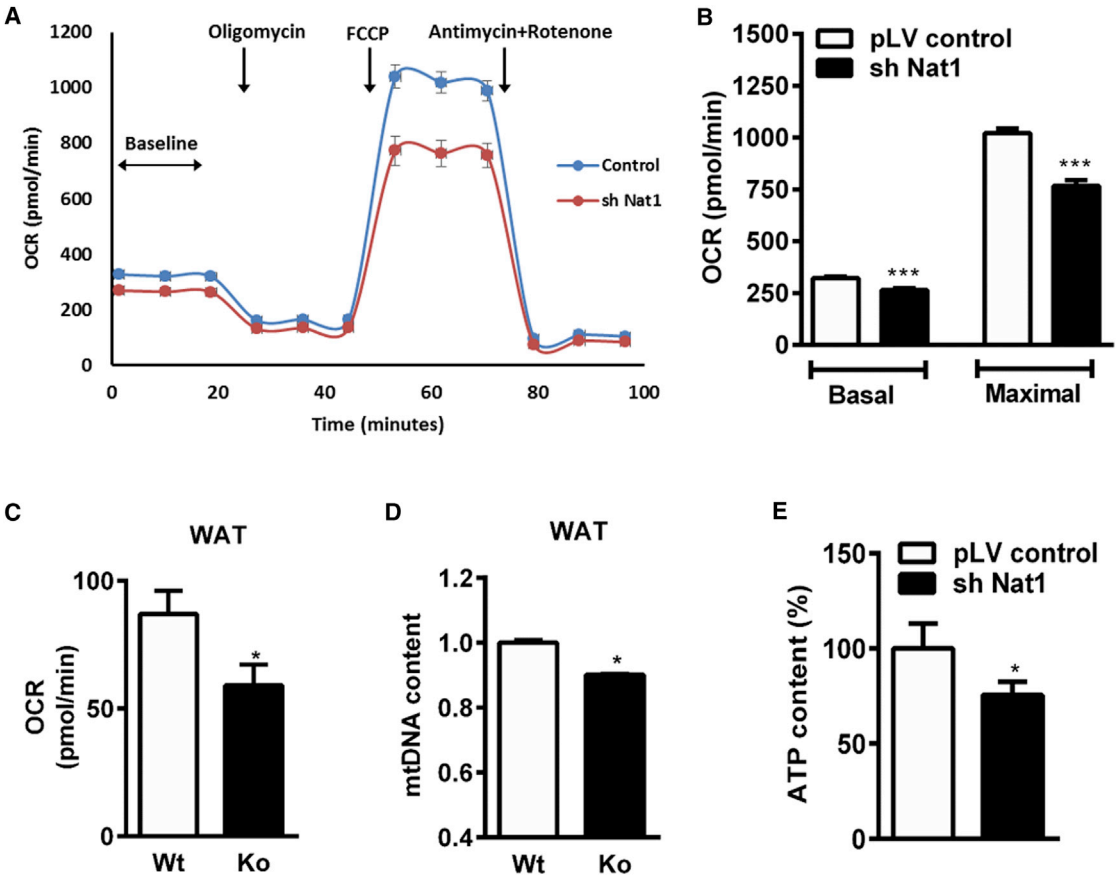

Figure 5. Effect of *Nat1* Ablation on Cellular Respiration and ATP Production in Differentiated 3T3-L1 Adipocytes

(A) Oxygen consumption rate (OCR) was measured using the XF24 Extracellular Fluid Analyzer in 3T3-L1 adipocytes transduced with control pLV and sh *Nat1*.

(B) Basal respiration and maximal respiration rates were determined from (A) (n = 9–10; $^{**}p \leq 0.01$ and $^{***}p < 0.001$).

(C and D) OCR (C) and mtDNA content (D, mtDNA/nDNA) were measured in WAT of WT and *Nat1*-deficient mice (n = 5; $^{*}p \leq 0.05$).

(E) Cellular ATP levels were measured in 3T3-L1 adipocytes. Data are presented as mean ± SEM of three separate experiments, with five wells per experiment ($^{*}p \leq 0.05$).

mice compared to WT controls, thus indicating a decreased number of mitochondria in the WAT of *Nat1* KO mice, which is consistent with decreased mitochondrial mass and biogenesis in 3T3-L1 adipocytes lacking *Nat1* expression (Figure 5D).

These data suggest that the inhibition of *Nat1* is associated with impaired cellular respiration. Given that respiration was significantly affected by *Nat1* deficiency, we next assessed the cellular ATP concentrations, and we found that *Nat1* knockdown in 3T3-L1 adipocytes resulted in a decrease of total cellular ATP levels by 24%, suggesting that the loss of *Nat1* markedly decreased overall mitochondrial function and ATP generation (Figure 5E).

Nat1 KO Mice Display Decreased Metabolic Rate and Energy Expenditure

Given the effect of *Nat1* on mitochondrial function and the observed effect on plasma metabolites and lipids, we hypothesized that *Nat1* deficiency would be associated with changes in basal metabolic rate. To better understand the role of *Nat1* in whole-body energy expenditure under basal conditions, we subjected 4-month-old WT and *Nat1*-deficient mice fed a normal chow diet to indirect calorimetry analysis in metabolic cages for 24 hr. *Nat1* KO mice exhibited increased respiratory exchange ratio (RER) (Figure 6A) and decreased whole-body OCR (VO2) (Figure 6B), suggesting an inability to switch from carbohydrate to fat metabolism. Overall resting energy expenditure was significantly decreased in *Nat1* KO mice compared to WT mice (Figure 6C).

Nat1-Deficient Mice Are Cold Tolerant

Given that *Nat1* deficiency was associated with changes in basal metabolic rate, a reasonable hypothesis is that *Nat1* deficiency also would have a primary effect on thermogenesis. Therefore, we assessed fuel metabolism by indirect calorimetry for 24 hr. Heat production was measured in 4-month-old WT and *Nat1*-deficient mice fed a normal chow diet for 24 hr. Over the course of 24 hr, the percentage of energy generated from fatty acid oxidation was less than carbohydrate metabolism in *Nat1* KO mice (Figures 6D and 6E).

Brown adipose tissue (BAT) is involved in the generation of heat by burning lipids. BAT is activated during cold exposure

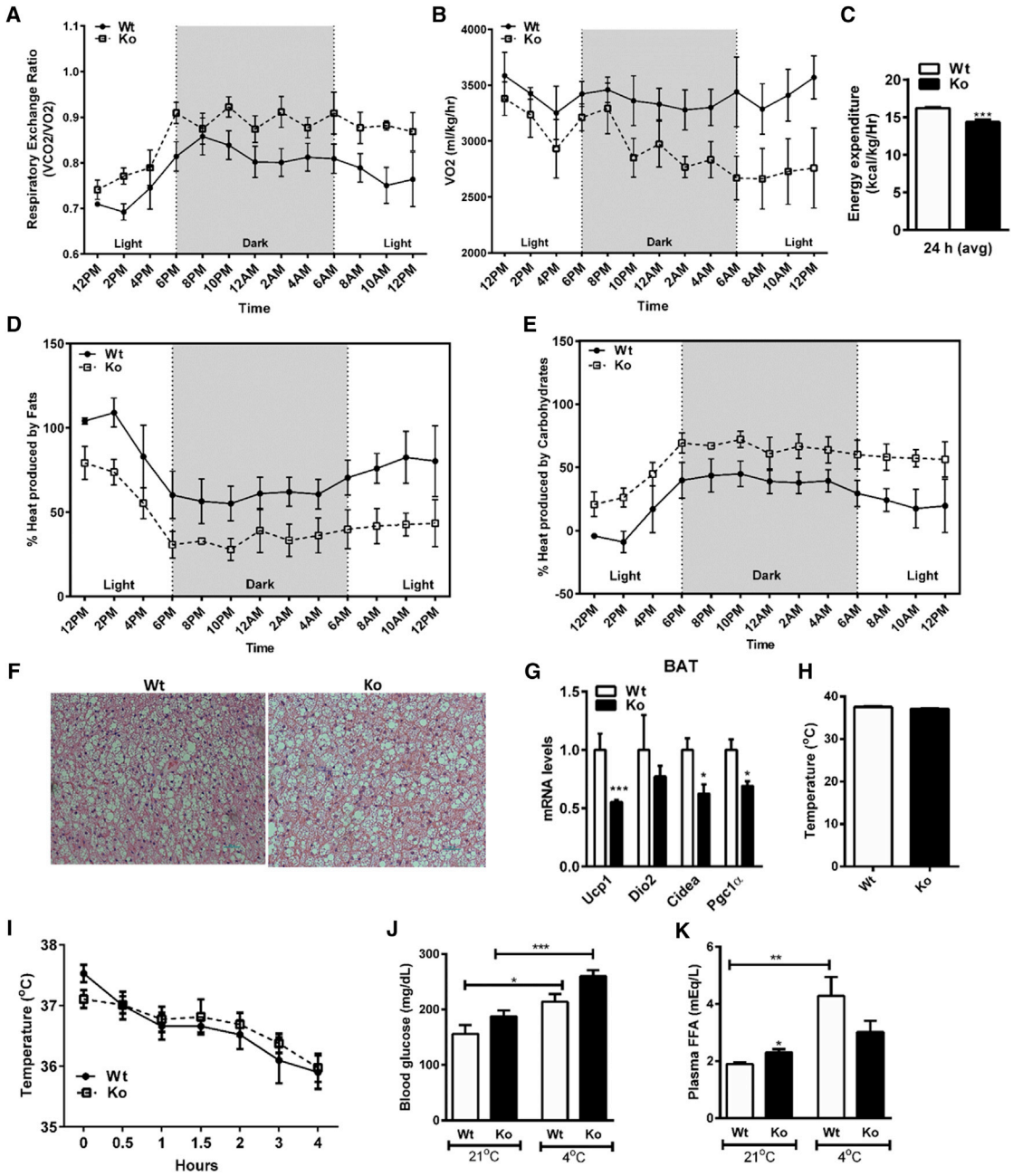

Figure 6. Decreased Metabolic Rate in *Nat1* KO Mice

(A–C) RER (A), VO2 (B), and energy expenditure (C) were measured in 4-month-old WT and *Nat1*-deficient mice given a normal chow diet for 24 hr (n = 4 mice per group; ***p $\leq$ 0.001).

(D and E) Heat production was measured for 24 hr in 4-month-old WT and *Nat1*-deficient mice given a normal diet for 24 hr (n = 4).

(F) H&E staining of BAT of WT and *Nat1*-deficient mice (n = 4) is shown.

(G) Thermogenic gene expression in BAT of WT and *Nat1*-deficient mice (n = 3), normalized to cyclophilin. Results represent mean ± SEM.

(H) Core body temperature was measured in 4-month-old WT and *Nat1*-deficient male mice fed a chow diet (n = 5–8 mice).

(I) Rectal temperature was measured every 30 min for 4 hr after exposure to a 4°C environment (n = 5–8 mice).

(J and K) Blood glucose (J) and non-esterified fatty acids in plasma (K) were measured in WT and *Nat1*-deficient mice (*p $\leq$ 0.05, **p $\leq$ 0.01, and ***p $\leq$ 0.001).

to maintain core body temperature. Histological analysis of BAT from WT and *Nat1* KO mice did not show differences in lipid accumulation under basal conditions (Figure 6F). However, ablation of *Nat1* resulted in reduced expression of the major thermogenic genes, including *Pgc1a*, uncoupling protein 1 (*Ucp1*), and cell death-inducing DFFA-like effector A (*Cidea*) (Figure 6G). We also assessed their basal core body temperature and found no difference between the WT and *Nat1*-deficient mice (Figure 6H).

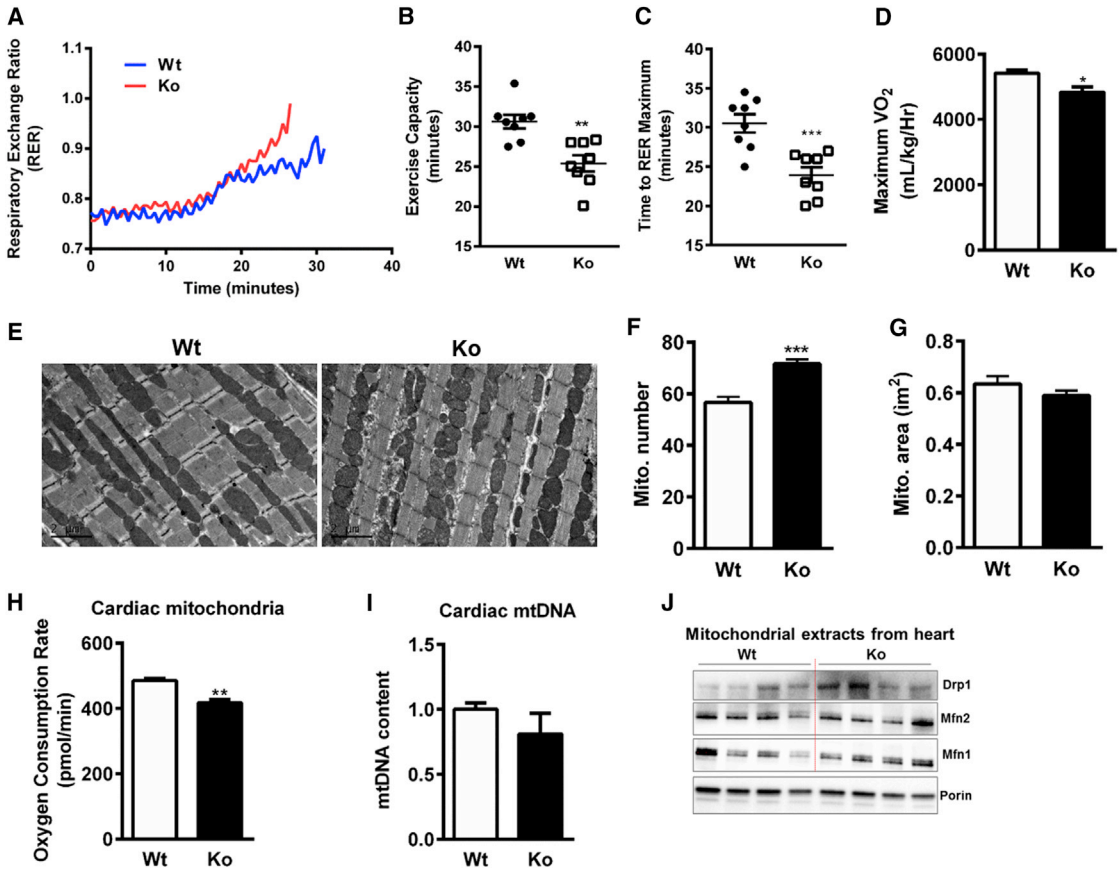

Figure 7. *Nat1* Deficiency on Energy Expenditure and Cardiac Phenotype In Vivo

(A–D) Mean RER (A), exercise capacity (B), time to exhaustion (C), and baseline and maximal VO2 were determined during exercise by treadmill protocol. Values are the means ± SEM of n = 8 mice per group (*p ≤ 0.05, **p ≤ 0.01, and ***p ≤ 0.001).

(E) Representative electron micrographs show the hearts of 4-month-old mice. Scale bar, 2 μm.

(F and G) Mitochondrial number and area were quantified blindly from eight to ten images from different fields (n = 4; ***p ≤ 0.001).

(H) OCR of heart-isolated mitochondria was assessed using an Oroboros Oxygraph-2k respirometer (n = 5–7 mice per group; **p ≤ 0.01).

(I) Relative mtDNA content was measured in cardiac muscle of WT and Nat1-deficient mice (n = 3).

(J) Mitochondrial markers in isolated mitochondrial fractions from hearts of WT and *Nat1*-deficient mice (n = 4) are shown.

To investigate a possible role for *Nat1* in BAT function, we exposed *Nat1* KO and WT mice to a cold (4°C) environment for 4 hr in order to activate BAT. Rectal temperature was measured every 30 min. The *Nat1*-deficient mice had no difference in core body temperature following cold exposure compared to WT mice (Figure 6I). Circulating glucose and FFAs also were measured before and after the cold challenge. *Nat1*-deficient mice exhibited a marked increase in blood glucose levels but no change in the plasma FFAs after cold exposure (Figures 6J and 6K). Together, these results suggest that *Nat1* deficiency is associated with a preferential use of carbohydrates over fats as fuel both under basal and cold-challenge conditions and potentially a reduction in FFA release.

Nat1 Deletion Impairs Exercise Capacity and Cardiac Mitochondrial Respiration in *Nat1* KO Mice

Given that mitochondrial function is a key determinant of exercise capacity, we sought to evaluate whether *Nat1* deficiency would be accompanied by decreased exercise tolerance. We subjected 12- to 14-week-old *Nat1* KO and WT littermate mice on a normal chow diet to a treadmill exercise challenge. *Nat1*-deficient animals exhibited a 19% decrease in exercise capacity, a 23% decrease in time to exhaustion, a lower anaerobic threshold, and a 14% decrease in VO2 maximum compared to their WT controls (Figures 7A–7D).

To examine the possibility that the decreased exercise capacity in *Nat1*-deficient mice can be attributed to effects on cardiac mitochondria, we performed electron microscopic analyses of heart tissue, which showed smaller mitochondria in *Nat1* KO mice compared with WT mice (Figures 7E–7G). Lipid droplets were present among mitochondria in KO mice (data not shown). Oxygen consumption was significantly decreased in cardiac mitochondria from *Nat1* KO mice versus control mice (Figure 7H). However, no changes were observed in the mitochondrial DNA content (Figure 7I). We also measured mitochondrial markers in isolated mitochondrial fractions from hearts. *Nat1* KO mice exhibited increased expression of mitochondrial fission marker Drp1 (Figure 7J).

We also examined cardiac function in *Nat1* KO and WT mice in the resting state with echocardiography. There was no change in left ventricular internal diameter (LVID) or percentage fractional shortening (FS%) in the *Nat1* KO mice compared with control animals (Figure S6). All echocardiography measurements are shown in Table S3.

Given that skeletal muscle is also a major determinant of energy expenditure, we assessed whether global deficiency of *Nat1* is associated with functional defects in skeletal muscle mitochondrial function. C2C12 myoblasts with *Nat1* knockdown had significantly decreased cellular respiration (Figure S7A). Furthermore, *Nat1* KO mice exhibited smaller and increased numbers of mitochondria per tibialis muscle fiber (Figures S7B–S7D) and increased expression of mitochondrial fission marker Drp1 compared to the WT mice (Figure S7E).

DISCUSSION

Our findings link deficiency of the IR gene *Nat1* to profound mitochondrial dysfunction characterized by an enhanced accumulation of ROS and superoxides (O_2^-), an increase in mitochondrial membrane depolarization, decreased basal and maximal cellular respiration, and decreased ATP production. Though our most detailed characterization was performed in 3T3-L1 adipocytes and WAT, the major observations of mitochondrial dysfunction were extended to skeletal muscle cells (C2C12 myoblasts) and tissue as well as cardiac cells. In addition, our in vivo observations suggest that mitochondrial dysfunction seen in *Nat1* KO mice is accompanied by a decrease in basal respiration and exercise capacity. Finally, multiple lines of evidence suggest a dysregulation in the ability to utilize fats for energy.

Thus, this study provides a specific genetic mechanism (*Nat1* deficiency) that may help explain prior observations that tied mitochondrial dysfunction and impaired biogenesis with IR and abnormal glucose homeostasis (Handschin et al., 2007; Johnson and Olefsky, 2013; Kelley et al., 2002; Kim et al., 2000; Kleiner et al., 2012; Morino et al., 2006; Petersen et al., 2004; Schrauwen and Hesselink, 2004; Vianna et al., 2006). Furthermore, our findings also suggest a means to partly explain the co-occurrence of mitochondrial dysfunction in adipose tissue in animal models of T2D as well as in human obesity, T2D, and the metabolic syndrome (Bogacka et al., 2005a, 2005b; Choo et al., 2006; Patti and Corvera, 2010).

This mitochondrial dysfunction could be due to decreased mitochondrial number/mass or decreased mitochondrial efficiency. Our results suggest that both of these processes are affected by *Nat1* deficiency. Mitochondrial mass was markedly reduced as were master regulators of mitochondrial biogenesis and function, such as *Pgc1a* and *Pgc1b*, nuclear respiratory factor 1 (*Nrf1*), and mitochondrial transcription factor A (*Tfam*). Mitochondria constantly fuse and divide, processes known as fusion and fission, and excessive mitochondrial fragmentation induces mitochondrial dysfunction. In our study, we observed a significant increase in mitochondrial fragmentation and *Drp1* expression in *Nat1* KO cells compared to the controls, indicating that the deficiency of *Nat1* triggers mitochondrial fragmentation by increasing *Drp1*. In addition, selective thermogenic genes in BAT were significantly decreased in *Nat1*-deficient mice compared with WT controls, which also may reflect effects on *Pgc1a*. Finally, key parts of the electron transport chain and ATP generation, e.g., *Cycs*, were significantly downregulated in *Nat1*-deficient cells and WAT.

Nat1-associated mitochondrial dysfunction may be primary or secondary (for instance, related to mitochondrial substrate availability). While the former is likely, as outlined above, it is difficult to exclude the latter. As an example, we found that fasted *Nat1* KO mice have markedly reduced levels of multiple plasma acylcarnitines. Acylcarnitines result from the addition of a carnitine molecule to an activated FFA, a prerequisite for FFA to be transported into the mitochondria and undergo β-oxidation. Together with the fact that *Nat1* KO mice have an inability to utilize fatty acids, it suggests that *Nat1* deficiency is associated with an impaired fatty acid transportation and/or β-oxidation. The resulting diminution in acylcarnitines is a common feature of IR (Noland et al., 2009). However, it is not yet clear whether acylcarnitines are reflecting or inflicting IR (Schooneman et al., 2013).

Nat1 deficiency is also associated with the reduction of numerous lysophospholipids, phospholipids, glycerolipids, and amino acids that are consistent with an IR phenotype (Roberts et al., 2014). Interestingly, deregulated lipids often contain linoleic acid 18:2. LPC (18:2) is a well-known negative correlate of IR, dysglycemia, and diabetes (Ferrannini et al., 2013; Floegel et al., 2013; Gall et al., 2010; Wang-Sattler et al., 2012), and LPCs have been shown to be reduced in obesity and T2D (Kim et al., 2011, 2013; Wang-Sattler et al., 2012). The global decrease of phospholipids may be due to a reduced biosynthesis, because phospholipid precursors choline, phosphorylcholine, and sn-glycero-3-phosphoethanolamine also were found in lower quantities in the plasma of *Nat1* KO mice.

The arginine and proline metabolism (L-aspartic acid, L-arginine, creatine, ornithine, L-proline, and L-glutamic acid) pathway was the most significantly deregulated upon *Nat1* depletion. Most of these metabolites have been associated with obesity and diabetes (Giesbertz et al., 2015). We also found a reduction in the quantity of glycine in *Nat1* deficiency that is a well-established negative correlate to diabetes and obesity (Ferrannini et al., 2013; Giesbertz et al., 2015; Newgard et al., 2009; Wang-Sattler et al., 2012). Altogether these results suggest that *Nat1* deficiency destabilizes energy homeostasis.

This altered homeostasis also is manifested in other ways. *Nat1*-deficient mice accumulate more fat in the form of WAT depots and liver TG without a change in daily food intake or changes in FFA levels or expression levels of genes involved in lipogenesis, which include fatty acid synthase (*Fas*) and sterol regulatory element-binding protein 1 (*Srebp1*). The increased adiposity could reflect a decrease in energy expenditure. In this regard, we observed that *Nat1* deficiency significantly decreased the expression of *Ucp1* and related thermogenic genes (*Cidea* and *Pgc1a*) in BAT, suggesting decreased thermogenesis (Enerbäck et al., 1997; Matthias et al., 2000; Ricquier and Bouillaud, 2000; Wolf, 2009) and Ucp1 ablation, which induces obesity (Feldmann et al., 2009). *Nat1* KO mice also seem to derive less heat from fatty acid oxidation. Assessment

of the animals' responses to acute cold exposure showed that the *Nat1* KO mice have a diminished FFA response but a more profound elevation in glucose compared to WT mice. However, these experiments did not reveal any gross thermogenic impairment in the *Nat1* KO mice, as they maintained their core body temperature equal to WT mice.

Such an acute challenge of mice previously housed at room temperature triggers a response in which all available heat-generating tissues are maximally activated. In such animals this consists of a combination of shivering (muscle dependent) and previously adapted uncoupled thermogenesis (BAT dependent) (Cannon and Nedergaard, 2011). While our cold challenge data do not distinguish between the relative contribution of muscle and BAT to the maintenance of heat, they strongly suggest that a primary defect in the thermogenic capacity or functionality of BAT is not causative of the change in energy balance observed in the *Nat1* KO mice. Such severe impediments to BAT thermogenesis usually result in a more marked drop in core body temperature following this type of challenge (Lee et al., 2015). Subtler impairments to the efficiency of BAT or compensatory increases in muscle-shivering capacity, caused by the previously highlighted changes to substrate availability and with the potential to impact energy balance, cannot be ruled out. However, longer-term chronic cold exposure and perhaps tissue-specific KO models would likely be required to dissect such adaptive changes in the *Nat1* KO mouse.

A key finding in the current study is that WT mice run longer than *Nat1*-deficient mice. The decreased endurance in *Nat1*-deficient mice is accompanied by decreased VO2. Decreased exercise endurance in *Nat1*-deficient mice suggests reduced oxygen-dependent respiration during exercise. This is supported by the fact that *Nat1*-deficient mice reach anaerobic threshold sooner than the control mice (Figure 7C).

Impaired exercise capacity is a predictor of IR, T2D, cardiovascular diseases, and overall mortality (Church et al., 2004; Fang et al., 2005), and mitochondria play a key role in the response to exercise challenge. The mitochondrial dysfunction seen in *Nat1* deficiency is likely contributing to the observed decreased exercise capacity in *Nat1* KO mice (Figure 7). Furthermore, *Nat1* KO mice also had a higher resting RER and decreased basal energy expenditure versus WT mice (Figure 6), suggesting that *Nat1* deficiency may involve preferential use of inefficient carbohydrate over fats as fuel during resting and active states. Our observations linking *Nat1* deficiency to insulin sensitivity, mitochondrial function, and exercise capacity demonstrate the interconnectedness of these phenotypes.

In conclusion, our data reveal a metabolic function of *Nat1* that triggers mitochondrial dysfunction and is accompanied by changes in cellular respiration that are correlated at a whole-body level with decreased basal energy expenditure and exercise tolerance. These findings shed light on the cellular mechanistic link among *Nat1*, IR, and mitochondrial function. Additional research may identify new treatment approaches targeting mitochondria. The link between insulin sensitivity and mitochondria may be a fruitful area of discovery as new IR loci are being identified.

EXPERIMENTAL PROCEDURES

Animals

Nat1-targeted mice (*Nat1* KO) were produced as described previously (Knowles et al., 2015). Mice were housed in a pathogen-free barrier facility with a 12-hr light/dark cycle, and they were fed standard rodent chow diet and water ad libitum. Male mice between 3 and 4 months old were used in all the experiments.

Systemic Metabolic Parameters

Overnight fasting blood samples were collected by retro-orbital bleeding from anesthetized mice and EDTA plasma was prepared immediately. Plasma concentrations of adiponectin (Crystal Chem), leptin (Crystal Chem), insulin (Crystal Chem), and FFA (Wako Diagnostics) were determined enzymatically according to the manufacturers' protocols. Overnight fasting blood glucose levels from the tail vein were measured with a glucometer (TRUEbalance, Nipro Diagnostics).

Study Approval for Animal Work

All animal protocols were approved by the Administrative Panel on Laboratory Animal Care at Stanford University, and they were performed in accordance with the guidelines of the American Association for the Accreditation of Laboratory Animal Care.

Histology

Histological analysis was performed according to standard protocols for paraffin-embedded samples.

Cell Culture

The murine 3T3-L1 and C2C12 myoblasts were obtained from American Type Culture Collection, cultured and differentiated according to the manufacturer's instructions. Details are given in the Supplemental Experimental Procedures.

Nat1 Knockdown Using siRNA in 3T3-L1 Adipocytes

For knockdown experiments, differentiated 3T3-L1 adipocytes were transfected with 50 nM synthetic predesigned small interfering RNA (siRNA) targeting *Nat1* or non-silencing siRNA (scr siRNA) (OriGene) using lipofectamine 2000 transfection reagent (Life Technologies), following the manufacturer's recommended protocol. After 48 hr of transfection, the media were changed.

Nat1 Knockdown Using Lentiviral Constructs

Cells were transduced with a combination of lentiviral particles for two knockdown constructs at an MOI of 100 each. After overnight incubation, medium containing viral particles was removed and replaced with fresh medium. The transduction efficiency was assessed by quantifying the percentage of GFP-positive cells by flow cytometry on a BD FACS Calibur. *Nat1* knockdown efficiency was confirmed by qPCR.

RNA Extraction, Reverse Transcription, and Real-Time PCR

RNA extraction, reverse transcription, and real-time PCR were performed as described in the Supplemental Experimental Procedures. Primer sequences are given in Table S3. The gene expression values were normalized to cyclophilin A as a housekeeping gene. The data were analyzed by the public domain program Relative Expression Software Tool – REST. Values are presented as mean ± SEM (Chennamsetty et al., 2011).

Protein Extraction and Immunoblotting

Immunoblotting was performed as described in the Supplemental Experimental Procedures. The primary antibodies used were as follows: LC3A/B (Cell Signaling Technology), Porin/anti VDAC1 (Abcam), Drp1 (BD Transduction Laboratories), Pgc1a (H 300), PINK1, β-actin (Santa Cruz Biotechnology), Mfn1 (Abcam), and Mfn2 (Abnova).

Intracellular ROS

Intracellular ROS generation was determined using H2DCFDA (10 μM, Sigma-Aldrich), as per the manufacturer's protocol. In brief, adipocytes were washed and incubated with H2DCFDA for 20 min. Cells were then washed twice gently,

and fluorescence was measured using a microplate reader (Tecan) with excitation/emission wavelengths of 485/515 nm.

Mitochondrial Superoxide Measurement

MitoSOX Red (Molecular Probes) was used to measure mitochondrial specific superoxide. Cells were stained, washed twice with PBS, and live cell images were taken using a fluorescence microscope.

Mitochondrial Membrane Potential, $\Delta\Psi m$

Mitochondrial membrane potential was measured using a TMRM kit (Abcam). The 3T3-L1 cells in 96-well black-walled culture plates were incubated with 100 nM TMRM for 20 min at 37°C in PBS containing 0.2% BSA. After the cells were washed, the TMRM fluorescence was monitored using a fluorescent microscope and the cells were imaged. Membrane potential was further verified using a fluorescent plate reader (Tecan). The excitation and emission wavelengths were set at 445 and 580 nm, respectively.

ATP Production Assay

The ATP content of the adipocytes was measured using a Luminescent ATP Detection Assay Kit (PerkinElmer) according to the manufacturer's protocol. Cells were mixed with the detection reagent, and luminescence was measured, using a 10-s integration time with a microplate luminometer and SOFTmax PRO software (Molecular Devices), and normalized to protein concentration.

mtDNA Content

Genomic DNA was isolated from tissues of WT and *Nat1* KO mice (n = 5 per group) using the DNeasy Blood & Tissue Kit (QIAGEN), following the manufacturer's instructions. The mtDNA content was assessed by real-time qPCR. The relative mtDNA content was evaluated by the ratio of DNA levels between mitochondrial Cox1 and nuclear 18S rRNA.

Mitochondrial Mass Measurement

3T3-L1 adipocytes were incubated with 50 nM MitoTracker Deep Red FM (Invitrogen) in serum-free DMEM for 30 min at 37°C. Cells were then washed thoroughly with PBS, trypsinized, centrifuged, and resuspended in PBS. Fluorescent intensity was analyzed using a FACS Calibur (BD Pharmingen).

Confocal Laser Microscopy for Visualizing Mitochondria

3T3-L1 adipocytes were transduced with lentivirus for controls and sh Nat1 was stained with mitochondria-specific fluorescent dye, MitoTracker Red CMXRos (100 nM), then fixed in 4% paraformaldehyde, and mitochondria were visualized by confocal microscopy and analyzed for area, perimeter, circularity, and interconnectivity by ImageJ.

XF24 Oxygen Consumption Assay and Bioenergetics Profile

Oxygen consumption was measured using the XF24 extracellular flux analyzer from Seahorse Bioscience according to their protocol. Cells were seeded in a 24-well XF24 cell culture microplate (Seahorse Bioscience) at a density of 10,000 cells per well in 200 μl DMEM supplemented with 10% fetal bovine serum (FBS). Cells were differentiated. The rate of oxygen consumed by the cells as an indicator of mitochondrial respiration was measured using XF cell mito stress test kit (Seahorse Bioscience), as per the manufacturer's instructions. Three basal OCR measurements were performed using the Seahorse analyzer, and measurements were repeated following the injection of oligomycin, FCCP, and rotenone/antimycin A. Basal ECAR was determined from data collected at basal measurement points.

Measurement of Endogenous Respiration Using Oxygraph 2K

Isolated mitochondria and tissues were used for oxygraphic measurements (Oxygraph 2K; Oroboros Instruments) according to the manufacturer's protocol. The rate of oxygen consumed was recorded. Respiration rates were normalized to total protein content.

Mitochondrial Isolation

Mitochondria were isolated from 3T3-L1 adipocytes and tissues using Mitochondria Isolation Kit according to the manufacturer's protocol (Abcam).

Metabolic Expenditure Measurements

For basal metabolic expenditure measurements, mice were placed in an Oxymax metabolic Chamber (Columbus Instruments), and oxygen consumption (VO2) and carbon dioxide expiration (VCO2) were measured using an open-circuit volumetric method of gas analysis (Desai et al., 1997). RER was calculated as VCO2/VO2. The rate of basal metabolic expenditure (BME) was calculated using the subjects VO2 * calorific value (CV), which is the relationship between heat and the volume of consumed oxygen. CVs are derived from historical empirical data. BME was then normalized to whole-body weight (kg). Analysis of the oxidation of carbohydrates and fats was calculated as previously published.

Body Temperature and Cold Exposure

Body temperatures were assessed in 4-month-old mice using a RET-3 rectal probe for mice (Physitemp). For the cold-exposure experiment, mice were housed individually and transferred to a cold room with an ambient temperature of 4°C. Temperature was measured every 30 min for 4 hr or until mouse core body temperature dropped below 25°C.

Triglyceride Quantification

Frozen liver tissue (50 mg) was homogenized and total lipids were extracted by the Folch method. Lipids were dried and reconstituted by brief sonication in 0.1% Triton X-100. TG content was quantified by using enzymatic assays (Wako Pure Chemicals Industries).

Animal Exercise Protocol

Mice were exercised on a treadmill equipped for simultaneous measurement of O2 consumption (VO2) and CO2 production (VCO2) (Columbus Instruments), and distance run, total work, and RER were determined using established protocols (Desai et al., 1997). Exercise capacity was assessed using a protocol that incrementally increased the degree of elevation of the treadmill by 2° and the speed by 2 m/min every 3 min. Mice were exercised until exhaustion while monitoring VO2/CO2. Mice were not forced to exercise after exhaustion.

Echocardiographic Assessment of Cardiac Function

Resting in vivo heart function was evaluated by echocardiography at 14–15 weeks. Mice were anesthetized with isoflurane (2% inhalation). 2D clips and M-mode images were obtained in the short-axis view from the mid-left ventricle (mid-LV) at the tips of the papillary muscles with a Sonos 5500 echocardiograph (Philips). Details are given in the Supplemental Experimental Procedures.

Non-targeted Metabolomic and Lipidomic Experiments by Liquid Chromatography-Mass Spectrometry

Metabolites were extracted from mouse plasma as described previously (Contrepois et al., 2015), and lipids were extracted using the Folch method with some modifications. Pathway analysis was performed using the metabolites with a Human Metabolome Database (HMDB) accession number in the web tool Metaboanalyst (Xia et al., 2015). Details are given in the Supplemental Experimental Procedures.

Generation of B6 × BTBR Cross F2 Mice and Genotyping and Gene Expression Data

Construction of the diabetes-segregating F2 cohort has been described previously (Tian et al., 2015; Tu et al., 2012). Details are given in the Supplemental Experimental Procedures.

Analysis of *Nat1*-Correlated Gene Sets

GO and KEGG pathway enrichment analyses were performed using the DAVID bioinformatic database at the NIH (https://david.ncifcrf.gov/). The 500 most correlated genes to *Nat1* (both positive and negative correlates) were identified from ~500 adipose samples from the F2 mice described above. The correlated gene sets were uploaded to DAVID, resulting in the GO and KEGG enrichments presented in Table S1. Mitochondrial genes were identified from the mouse MitoCarta database at the Broad Institute (http://www.broadinstitute.org/files/shared/metabolism/mitocarta/mouse.mitocarta.2.0.html). The mitochondrial

genes showing the strongest positive correlation to the adipose expression of Nat1 are given in Table S1.

Statistical Analyses

Statistical analyses of the experiments were performed with GraphPad Prism 5.0. Two-tailed unpaired Student's t test and ANOVA were applied to determine statistical significance (*$p \leq 0.05$, **$p \leq 0.01$, and ***$p \leq 0.001$).

SUPPLEMENTAL INFORMATION

Supplemental Information includes Supplemental Experimental Procedures, seven figures, and four tables and can be found with this article online at http://dx.doi.org/10.1016/j.celrep.2016.09.005.

AUTHOR CONTRIBUTIONS

I.C. contributed to basic science experiments in vitro and in vivo and writing the manuscript. M.C. contributed to the mitochondrial experiments, helped write sections of the manuscript, and provided critical comments. K.C. contributed to the generation and analysis of metabolomics and lipidomics data, helped write sections of the manuscript, and provided critical comments. M.P.K. contributed to co-expression gene networks analysis, helped write sections of the manuscript, and provided critical comments. I.C.-O., G.F., A.J.W., and M.F. contributed to basic science experiments. J.S. contributed to basic science experiments in vivo. M.S., G.R., and T.Q. contributed to study design, discussion, and manuscript preparation. A.D.A. contributed to co-expression gene networks analysis and provided helpful comments and critical review of manuscript. D.B. contributed to the mitochondrial experiments in vitro and in vivo and also provided critical comments on the manuscript. J.W.K. conceived the work, contributed to the overall design, and helped write the manuscript.

ACKNOWLEDGMENTS

J.W.K. was supported by an American Heart Association Fellow-to-Faculty Transition Award (10FTF3360005) and by NIH grant U01HL107388. T.Q. was supported by NIH grants (U01HL107388, HL109512, and R21HL120757) and a grant from the LeDucq Foundation. M.C. was supported by NIH K99 award HL12947401A1. K.C. was supported by NIH grant 3U54DK10255603S1. I.C.-O. was supported by NIH grant U01HL107388. D.B. was supported by NIH grant HL061535. The authors thank Erik Ingelsson and Mark Walker for helpful comments.

Received: January 25, 2016
Revised: July 28, 2016
Accepted: August 31, 2016
Published: October 4, 2016

REFERENCES

Bogacka, I., Ukropcova, B., McNeil, M., Gimble, J.M., and Smith, S.R. (2005a). Structural and functional consequences of mitochondrial biogenesis in human adipocytes in vitro. J. Clin. Endocrinol. Metab. *90*, 6650–6656.

Bogacka, I., Xie, H., Bray, G.A., and Smith, S.R. (2005b). Pioglitazone induces mitochondrial biogenesis in human subcutaneous adipose tissue in vivo. Diabetes *54*, 1392–1399.

Cannon, B., and Nedergaard, J. (2011). Nonshivering thermogenesis and its adequate measurement in metabolic studies. J. Exp. Biol. *214*, 242–253.

Chennamsetty, I., Claudel, T., Kostner, K.M., Baghdasaryan, A., Kratky, D., Levak-Frank, S., Frank, S., Gonzalez, F.J., Trauner, M., and Kostner, G.M. (2011). Farnesoid X receptor represses hepatic human APOA gene expression. J. Clin. Invest. *121*, 3724–3734.

Choo, H.J., Kim, J.H., Kwon, O.B., Lee, C.S., Mun, J.Y., Han, S.S., Yoon, Y.S., Yoon, G., Choi, K.M., and Ko, Y.G. (2006). Mitochondria are impaired in the adipocytes of type 2 diabetic mice. Diabetologia *49*, 784–791.

Church, T.S., Cheng, Y.J., Earnest, C.P., Barlow, C.E., Gibbons, L.W., Priest, E.L., and Blair, S.N. (2004). Exercise capacity and body composition as predictors of mortality among men with diabetes. Diabetes Care *27*, 83–88.

Contrepois, K., Jiang, L., and Snyder, M. (2015). Optimized analytical procedures for the untargeted metabolomic profiling of human urine and plasma by combining hydrophilic interaction (HILIC) and reverse-phase liquid chromatography (RPLC)-mass spectrometry. Mol. Cell. Proteomics *14*, 1684–1695.

De Pauw, A., Tejerina, S., Raes, M., Keijer, J., and Arnould, T. (2009). Mitochondrial (dys)function in adipocyte (de)differentiation and systemic metabolic alterations. Am. J. Pathol. *175*, 927–939.

Desai, K.H., Sato, R., Schauble, E., Barsh, G.S., Kobilka, B.K., and Bernstein, D. (1997). Cardiovascular indexes in the mouse at rest and with exercise: new tools to study models of cardiac disease. Am. J. Physiol. *272*, H1053–H1061.

Disatnik, M.H., Ferreira, J.C.B., Campos, J.C., Gomes, K.S., Dourado, P.M.M., Qi, X., and Mochly-Rosen, D. (2013). Acute inhibition of excessive mitochondrial fission after myocardial infarction prevents long-term cardiac dysfunction. J. Am. Heart Assoc. *2*, e000461.

Dorn, G.W., 2nd. (2015). Mitochondrial dynamism and heart disease: changing shape and shaping change. EMBO Mol. Med. *7*, 865–877.

Enerbäck, S., Jacobsson, A., Simpson, E.M., Guerra, C., Yamashita, H., Harper, M.-E., and Kozak, L.P. (1997). Mice lacking mitochondrial uncoupling protein are cold-sensitive but not obese. Nature *387*, 90–94.

Facchini, F.S., Hua, N., Abbasi, F., and Reaven, G.M. (2001). Insulin resistance as a predictor of age-related diseases. J. Clin. Endocrinol. Metab. *86*, 3574–3578.

Fang, Z.Y., Sharman, J., Prins, J.B., and Marwick, T.H. (2005). Determinants of exercise capacity in patients with type 2 diabetes. Diabetes Care *28*, 1643–1648.

Feldmann, H.M., Golozoubova, V., Cannon, B., and Nedergaard, J. (2009). UCP1 ablation induces obesity and abolishes diet-induced thermogenesis in mice exempt from thermal stress by living at thermoneutrality. Cell Metab. *9*, 203–209.

Ferrannini, E., Natali, A., Camastra, S., Nannipieri, M., Mari, A., Adam, K.-P., Milburn, M.V., Kastenmüller, G., Adamski, J., Tuomi, T., et al. (2013). Early metabolic markers of the development of dysglycemia and type 2 diabetes and their physiological significance. Diabetes *62*, 1730–1737.

Floegel, A., Stefan, N., Yu, Z., Mühlenbruch, K., Drogan, D., Joost, H.-G., Fritsche, A., Häring, H.-U., Hrabě de Angelis, M., Peters, A., et al. (2013). Identification of serum metabolites associated with risk of type 2 diabetes using a targeted metabolomic approach. Diabetes *62*, 639–648.

Frayn, K.N. (2001). Adipose tissue and the insulin resistance syndrome. Proc. Nutr. Soc. *60*, 375–380.

Gall, W.E., Beebe, K., Lawton, K.A., Adam, K.-P., Mitchell, M.W., Nakhle, P.J., Ryals, J.A., Milburn, M.V., Nannipieri, M., Camastra, S., et al.; RISC Study Group (2010). α-hydroxybutyrate is an early biomarker of insulin resistance and glucose intolerance in a nondiabetic population. PLoS ONE *5*, e10883.

Giesbertz, P., Padberg, I., Rein, D., Ecker, J., Höfle, A.S., Spanier, B., and Daniel, H. (2015). Metabolite profiling in plasma and tissues of ob/ob and db/db mice identifies novel markers of obesity and type 2 diabetes. Diabetologia *58*, 2133–2143.

Handschin, C., Choi, C.S., Chin, S., Kim, S., Kawamori, D., Kurpad, A.J., Neubauer, N., Hu, J., Mootha, V.K., Kim, Y.-B., et al. (2007). Abnormal glucose homeostasis in skeletal muscle-specific PGC-1α knockout mice reveals skeletal muscle-pancreatic β cell crosstalk. J. Clin. Invest. *117*, 3463–3474.

Johnson, A.M.F., and Olefsky, J.M. (2013). The origins and drivers of insulin resistance. Cell *152*, 673–684.

Kelley, D.E., He, J., Menshikova, E.V., and Ritov, V.B. (2002). Dysfunction of mitochondria in human skeletal muscle in type 2 diabetes. Diabetes *51*, 2944–2950.

Kim, J.-Y., Hickner, R.C., Cortright, R.L., Dohm, G.L., and Houmard, J.A. (2000). Lipid oxidation is reduced in obese human skeletal muscle. Am. J. Physiol. Endocrinol. Metab. *279*, E1039–E1044.

Kim, J.-Y., van de Wall, E., Laplante, M., Azzara, A., Trujillo, M.E., Hofmann, S.M., Schraw, T., Durand, J.L., Li, H., Li, G., et al. (2007). Obesity-associated improvements in metabolic profile through expansion of adipose tissue. J. Clin. Invest. *117*, 2621–2637.

Kim, H.-J., Kim, J.H., Noh, S., Hur, H.J., Sung, M.J., Hwang, J.-T., Park, J.H., Yang, H.J., Kim, M.-S., Kwon, D.Y., and Yoon, S.H. (2011). Metabolomic analysis of livers and serum from high-fat diet induced obese mice. J. Proteome Res. *10*, 722–731.

Kim, M.J., Yang, H.J., Kim, J.H., Ahn, C.-W., Lee, J.H., Kim, K.S., and Kwon, D.Y. (2013). Obesity-related metabolomic analysis of human subjects in black soybean peptide intervention study by ultraperformance liquid chromatography and quadrupole-time-of-flight mass spectrometry. J. Obes. *2013*, 874981.

Kleiner, S., Mepani, R.J., Laznik, D., Ye, L., Jurczak, M.J., Jornayvaz, F.R., Estall, J.L., Chatterjee Bhowmick, D., Shulman, G.I., and Spiegelman, B.M. (2012). Development of insulin resistance in mice lacking PGC-1α in adipose tissues. Proc. Natl. Acad. Sci. USA *109*, 9635–9640.

Knowles, J.W., Xie, W., Zhang, Z., Chennamsetty, I., Assimes, T.L., Paananen, J., Hansson, O., Pankow, J., Goodarzi, M.O., Carcamo-Orive, I., et al.; RISC (Relationship between Insulin Sensitivity and Cardiovascular Disease) Consortium; EUGENE2 (European Network on Functional Genomics of Type 2 Diabetes) Study; GUARDIAN (Genetics UndeRlying DIAbetes in HispaNics) Consortium; SAPPHIRe (Stanford Asian and Pacific Program for Hypertension and Insulin Resistance) Study (2015). Identification and validation of N-acetyltransferase 2 as an insulin sensitivity gene. J. Clin. Invest. *125*, 1739–1751.

Lee, J., Ellis, J.M., and Wolfgang, M.J. (2015). Adipose fatty acid oxidation is required for thermogenesis and potentiates oxidative stress-induced inflammation. Cell Rep. *10*, 266–279.

Matthias, A., Ohlson, K.B.E., Fredriksson, J.M., Jacobsson, A., Nedergaard, J., and Cannon, B. (2000). Thermogenic responses in brown fat cells are fully UCP1-dependent. UCP2 or UCP3 do not substitute for UCP1 in adrenergically or fatty scid-induced thermogenesis. J. Biol. Chem. *275*, 25073–25081.

Morino, K., Petersen, K.F., and Shulman, G.I. (2006). Molecular mechanisms of insulin resistance in humans and their potential links with mitochondrial dysfunction. Diabetes *55* (*Suppl 2*), S9–S15.

Newgard, C.B., An, J., Bain, J.R., Muehlbauer, M.J., Stevens, R.D., Lien, L.F., Haqq, A.M., Shah, S.H., Arlotto, M., Slentz, C.A., et al. (2009). A branched-chain amino acid-related metabolic signature that differentiates obese and lean humans and contributes to insulin resistance. Cell Metab. *9*, 311–326.

Noland, R.C., Koves, T.R., Seiler, S.E., Lum, H., Lust, R.M., Ilkayeva, O., Stevens, R.D., Hegardt, F.G., and Muoio, D.M. (2009). Carnitine insufficiency caused by aging and overnutrition compromises mitochondrial performance and metabolic control. J. Biol. Chem. *284*, 22840–22852.

Patti, M.-E., and Corvera, S. (2010). The role of mitochondria in the pathogenesis of type 2 diabetes. Endocr. Rev. *31*, 364–395.

Petersen, K.F., Dufour, S., Befroy, D., Garcia, R., and Shulman, G.I. (2004). Impaired mitochondrial activity in the insulin-resistant offspring of patients with type 2 diabetes. N. Engl. J. Med. *350*, 664–671.

Reaven, G.M. (1988). Banting lecture 1988. Role of insulin resistance in human disease. Diabetes *37*, 1595–1607.

Ricquier, D., and Bouillaud, F. (2000). The uncoupling protein homologues: UCP1, UCP2, UCP3, StUCP and AtUCP. Biochem. J. *345*, 161–179.

Roberts, L.D., Koulman, A., and Griffin, J.L. (2014). Towards metabolic biomarkers of insulin resistance and type 2 diabetes: progress from the metabolome. Lancet Diabetes Endocrinol. *2*, 65–75.

Schooneman, M.G., Vaz, F.M., Houten, S.M., and Soeters, M.R. (2013). Acylcarnitines: reflecting or inflicting insulin resistance? Diabetes *62*, 1–8.

Schrauwen, P., and Hesselink, M.K.C. (2004). Oxidative capacity, lipotoxicity, and mitochondrial damage in type 2 diabetes. Diabetes *53*, 1412–1417.

Sivitz, W.I., and Yorek, M.A. (2010). Mitochondrial dysfunction in diabetes: from molecular mechanisms to functional significance and therapeutic opportunities. Antioxid. Redox Signal. *12*, 537–577.

Tian, J., Keller, M.P., Oler, A.T., Rabaglia, M.E., Schueler, K.L., Stapleton, D.S., Broman, A.T., Zhao, W., Kendziorski, C., Yandell, B.S., et al. (2015). Identification of the bile acid transporter Slco1a6 as a candidate gene that broadly affects gene expression in mouse pancreatic islets. Genetics *201*, 1253–1262.

Tu, Z., Keller, M.P., Zhang, C., Rabaglia, M.E., Greenawalt, D.M., Yang, X., Wang, I.M., Dai, H., Bruss, M.D., Lum, P.Y., et al. (2012). Integrative analysis of a cross-loci regulation network identifies App as a gene regulating insulin secretion from pancreatic islets. PLoS Genet. *8*, e1003107.

Vianna, C.R., Huntgeburth, M., Coppari, R., Choi, C.S., Lin, J., Krauss, S., Barbatelli, G., Tzameli, I., Kim, Y.-B., Cinti, S., et al. (2006). Hypomorphic mutation of PGC-1β causes mitochondrial dysfunction and liver insulin resistance. Cell Metab. *4*, 453–464.

Wang, Y., Rimm, E.B., Stampfer, M.J., Willett, W.C., and Hu, F.B. (2005). Comparison of abdominal adiposity and overall obesity in predicting risk of type 2 diabetes among men. Am. J. Clin. Nutr. *81*, 555–563.

Wang-Sattler, R., Yu, Z., Herder, C., Messias, A.C., Floegel, A., He, Y., Heim, K., Campillos, M., Holzapfel, C., Thorand, B., et al. (2012). Novel biomarkers for pre-diabetes identified by metabolomics. Mol. Syst. Biol. *8*, 615.

Weyer, C., Foley, J.E., Bogardus, C., Tataranni, P.A., and Pratley, R.E. (2000). Enlarged subcutaneous abdominal adipocyte size, but not obesity itself, predicts type II diabetes independent of insulin resistance. Diabetologia *43*, 1498–1506.

Wolf, G. (2009). Brown adipose tissue: the molecular mechanism of its formation. Nutr. Rev. *67*, 167–171.

Xia, J., Sinelnikov, I.V., Han, B., and Wishart, D.S. (2015). MetaboAnalyst 3.0–making metabolomics more meaningful. Nucleic Acids Res. *43*, W251–257.

Yip, J., Facchini, F.S., and Reaven, G.M. (1998). Resistance to insulin-mediated glucose disposal as a predictor of cardiovascular disease. J. Clin. Endocrinol. Metab. *83*, 2773–2776.